Applied Catalysis B: Environmental 121–122 (2012) 230–238

Contents lists available at SciVerse ScienceDirect

Applied Catalysis B: Environmental

journal homepage: www.elsevier.com/locate/apcatb

Kinetics of photocatalytic disinfection in TiO_2-containing polymer thin films: UV and visible light performances

Anna Kubacka*, Manuel Ferrer, Marcos Fernández-García**

Instituto de Catálisis y Petroleoquímica, CSIC, C/Marie Curie 2, 28049 Madrid, Spain

ARTICLE INFO

Article history:
Received 18 January 2012
Received in revised form 8 March 2012
Accepted 13 March 2012
Available online 17 April 2012

Keywords:
Photocatalysis
Titania
Anatase
Metal and oxide promotion
Silver
Copper
Zinc
EVOH polymer
Biocidal
Germicidal
EPR

ABSTRACT

The photocatalytic disinfection potential of TiO_2- and Cu-, Zn- and Ag-promoted TiO_2 embedded in polymer-based materials has been analyzed upon both ultraviolet and visible light excitations. A complete set of microorganisms including two Gram-negative (*Escherichia coli* and *Pseudomonas earuginosa*) and two Gram-positive (*Staphylococcus aureus* and *Enterococcus faecalis*) bacteria and a yeast (*Pichia jadinii*) was used throughout the study. This series covers clinically and food derived infection relevant pathogens. A kinetic modeling using an "adsorption Langmuir–Hinshelwood" type mechanism was used to interpret the disinfection tests and the performance of the different TiO_2 photo-biocide agents. The results clearly indicate that Ag- and Zn-containing materials are the most effective in all conditions tested (e.g. irrespective of the microorganism nature and light energy) and this seems intimately linked with intrinsic characteristics of the radical species reaching the surface of the polymer-oxide nanocomposite films as detected by electron paramagnetic resonance.

1. Introduction

Incorporation of titania in polymer matrices emerges as a successful technology to fight against biological risks and guarantee the safety of products related to foods/beverages packaging or containers for biomedical/pharmaceutical materials/devices [1]. TiO_2-anatase is by far the most widely used photocatalyst, being a wide band-gap (3.0–3.2 eV) semiconductor that under UV illumination generates energy-rich electron–hole pairs able to degrade cell components of microorganisms [1,2]. The limited absorbance power of anatase in the visible light electromagnetic region and, therefore, the scarce potential use of renewable energy sources as the sun and/or the possibility of using visible-light indoor sources for supplying energy to photokilling processes are main drawbacks to be solved.

Here, EVOH–TiO_2 (EVOH, ethylene–vinyl alcohol copolymer) composite films with potential use in the food packaging industry are considered [3,4]. We previously showed in this system that the whole external composite surface can become biocidal by charge carrier transfer (specifically holes) from the anatase to the polymer component [5]. This erases the need for anatase-microorganism contact and leads to non-contact, long lasting, highly active biocidal materials. Among the paths to optimize biocidal properties of anatase, modification by surface deposition of silver is a well known tool allowing visible absorption (in the 450–550 nm range) through the localized metal surface plasmon (LSP) as well as promoting charge separation by metal electron capture [6,7]. The oxide-anatase contact has been tried with a significant number of systems [6]. Among them Cu_2O/CuO [8] and ZnO [9] appear optimum choices for separating charge carrier upon UV/visible lights and thus to facilitate hole transit to the organic component in our nanocomposite films. Moreover, as the EVOH–TiO_2 generates unique interface electronic states active upon visible light [3], the presence of limited amounts of Ag, Cu or Zn species at the anatase surface has been shown to produce novel (e.g. non-present in the corresponding, isolated M-TiO_2 and EVOH systems) effects on (UV/visible) optical properties without altering other physicochemical properties [10].

This work attempts to analyze the potential biocidal action of the TiO_2-alone, and Ag-, Cu-, and Zn-containing phases jointly used with titania in polymer-based nano-composites. These materials were subjected previously to a full microscopy and spectroscopy

* Corresponding author.
** Corresponding author. Tel.: +34 915 85 49 39; fax: +34 915 85 47 60.
E-mail addresses: ak@icp.csic.es (A. Kubacka), m.fernandez@icp.csic.es, mfg@icp.csic.es (M. Fernández-García).

0926-3373/$ – see front matter © 2012 Elsevier B.V. All rights reserved.
doi:10.1016/j.apcatb.2012.03.016

characterization which was published elsewhere [10]. In this contribution we focus on using a kinetic approach based in the work of Marugán et al. [11] to investigate the disinfection behavior of the systems against a complete set of five microorganism including Gram-negative (*Escherichia coli* and *Pseudomonas aeruginosa*), Gram-positive (*Staphylococcus aureus* and *Enterococcus faecalis*) bacteria and a yeast (*Pichia jadinii*) under both UV and visible light excitations. This series covers cynically and food infection relevant pathogens [1]. The increasing complexity of the microorganisms and, particularly, of their cell walls will be used to test the importance of such parameter in the killing of microorganisms by a photo-elimination process. Moreover, the kinetic approach appears as a key piece for understanding the differential behavior observed among the different promoters of the titania photo-active material e under both UV and visible excitations. The analysis is completed with the help of the electron paramagnetic resonance technique in order to analyze the radical species responsible of the photo-disinfection process.

2. Experimental

Composites were prepared by a melting compounding method as described previously yielding 100 μm films. The inorganic materials were included in all cases to a 2 wt.% level. Such inorganic compounds are bare TiO_2 (anatase), and composite materials including Ag(0), Cu_2O and ZnO phases on the surface of titania according to physico-chemical characterization. These Ag, Cu and Zn phases were introduced to a 1 wt.% level of the inorganic component (0.02 wt.% of the polymer-based composite). Full description of the sample preparation procedure and physico-chemical characteristics of the films can be found in Ref. [10].

The microorganisms used in this study include *E. coli* 1337-H, *P. aeruginosa* strain PAO1, *E. faecalis* clinical isolate brs30 from human biliary, *S. aureus* 1341-H, and *P. jadinii* CECT 1062 and were obtained from the Spanish Type Culture Collection (CECT; http://www.uv.es/cect/) and the German Collection of Microorganisms and Cell Cultures (DSMZ, Braunschweig, Germany) and cultured and maintained according to the recommendations of the suppliers (see details in Ref. [4]). Cells were grown in 100 mL-flasks filled with 10 mL of the respective medium and subsequently used for photochemical cell viability assays. Aliquots of 1 mL from these suspensions were added to a 4 mL quartz cubic cell containing 1 mL of sterilized water and the corresponding film under continuous stirring (constant weight, ca. 10 mg and surface, 0.2 mm × 1 mm were used for all samples). The film-cell slurry was placed in the UV spectrometer chamber (UVIKON 930) and irradiated with a light at 280 (UV) and 500 (visible) nm for different time periods. The excitation line width is lower than 10 nm in all cases. As demonstrated by blank experiments, care was put of using a sub-lethal, maximum radiation energy fluence of ca. 1 kJ m^{-2} throughout the study (60 min). The four samples (EVOH–TiO_2 and Ag, Cu and Zn containing nanocomposites) together with a blank (EVOH) were measured using the same bacterium inoculum (10^{8-9} CFU mL^{-1}) for each microorganism tested. During irradiation and for different time intervals, aliquots of 100 μL were transferred to a 10 mL Luria Bertani (LB) broth test tube. The order of cell dilution at this stage was 10^{-2}. Loss of viability after each exposure time was determined by the viable count procedure on Luria Bertani agar plates after serial dilution (10^{-2} to 10^{-5}). All plates were incubated at 37 °C for 24 h after which they were scanned using a Bio-Rad Imaging System equipped with Analysis Software 4.6.5 (Bio-Rad) to enable enumeration of bacterial colonies among replicates. Data reported in this contribution are typically the average of four different experiments.

Modeling of the inactivation profiles was achieved using an approach grounded in a simplified (Langmuir–Hinshelwood-like multistep-type) reaction mechanism based in three parameters: kinetic (k) and pseudo-adsorption (K) constants and an inhibition coefficient (n) [11]. This model considers that microorganism death occurs via a sequential attack of photo-radicals by which "undamaged" (denoted as u in subsequent equations) cells become "damaged" (denoted as d) and eventually progress to an "inactivated" state [11]. This leads to two differential equations as:

$$\frac{dN_u}{dt} = -k\frac{KN_u^n}{1 + KN_u^n + KN_d^n}$$

$$\frac{dN_d}{dt} = k\frac{KN_u^n - KN_d^n}{1 + KN_u^n + KN_d^n}$$

We slightly modified this model by assuming a fast decay from "undamaged" to inactivated cells which would lead to a simplified mechanism with a single differential equation paralleling the one of a classical Langmuir–Hinshelwood mechanism:

$$\frac{dN_u}{dt} = -k\frac{KN_u^n}{1 + KN_u^n}$$

We designed Model 1 as the model with a single differential equation while Model 2 described the one having two differential equations. Numerical solution of the corresponding set of equations was achieved with a 5th order "adaptive size controlled" Runge–Kutta program, coupled to a Full Newton algorithm in order to ensure the solution of the corresponding non-linear fitting problem [12].

The electron paramagnetic resonance (EPR) measurements were done with a Bruker ER200D spectrometer operating in the X-band and calibrated with a DPPH standard. For the 5,5-dimethyl-1-pyrroline N-oxide (DMPO) spin trapping EPR experiments, the samples were suspended in water (at a concentration of 1 g l^{-1}) and were sonicated for 4 min. An aqueous solution (0.01 M) of DMPO spin trap (supplied by Sigma) was prepared and kept on ice during the whole set of experiments. Bidistilled water (Elix-10) was employed for these preparations. 100 μL of the solid suspension and 100 μL of the DMPO solution were mixed into an EPR flat quartz cell under atmospheric air and irradiated at different times, through a spectroscopic Pyrex glass filter with a cut-off at ca. 220 nm, with light excitation source identical to that employed for the photokilling tests, being then immediately transferred to the spectrometer cavity for EPR analysis. A small radical concentration decay (of ca. 5% on average) was observed in the dark during the course of spectrum recording. The latter were obtained at 298 K at ca. 9.75 GHz microwave frequency, 19.5 mW microwave power, 100 kHz modulation frequency, 1 G modulation amplitude and 2×10^5 spectrometer gain. No significant signal saturation was observed in those conditions. Blank experiments were also performed over mixtures of 100 μL of the DMPO solution and 100 μL of water to check the absence of radical formation in the absence of solid under the employed conditions.

Another set of experiments was performed at 77 K using a conventional spectroscopic quartz tube cell (4 mm o.d.) employed for studies of solid samples. Aliquots of the sample (between 20 and 30 mg) were thoroughly treated under high vacuum conditions at room temperature and then irradiated during 15 min at 77 K. Experiments followed with chemisorption of oxygen (upon introduction in the cell of a 50 μmol g^{-1} dose) at 77 K followed by UV or visible irradiation in the presence of oxygen at 77 K and final thorough outgassing at 77 K.

3. Results and discussion

Table 1 summarized result from previous works concerning the structural properties of the nanocomposite films [10]. The data indicate that presence of metal species at organic-inorganic interfaces alter the mean diameter of the titania aggregates, being this change relatively modest for Ag- and Zn-containing films and significantly more drastic for Cu ones. All metals improve, in any case, the inorganic dispersion into the polymer matrix and, consequently, increase the organic–inorganic interface contact area. The table also shows the structural characteristics of the organic phase (polymer crystal size and degree of crystallinity as it is a

Table 1
Characteristics of organic/inorganic crystalline phase for the different nanocomposites and for the EVOH polymer: f_c^{WAXS} (crystallinity degree determined by WAXS at room temperature); L: long spacing estimated by SAXS; l_c: most probable crystal size; S: aggregate size of the anatase component.[a]

System	L^{SAXS} (nm)	f_c^{WAXS}	l_c (nm)	S (nm)
EVOH	13.8	0.40	5.5	–
Ti	13.8	0.40	5.5	90
Ag	14.4	0.40	5.8	66
Cu	14.6	0.40	5.8	49
Zn	14.1	0.40	5.6	74

[a] Standard deviation (±): 7% for f_c^{WAXS}; 0.5 nm for L and l_c; 30 nm for S.

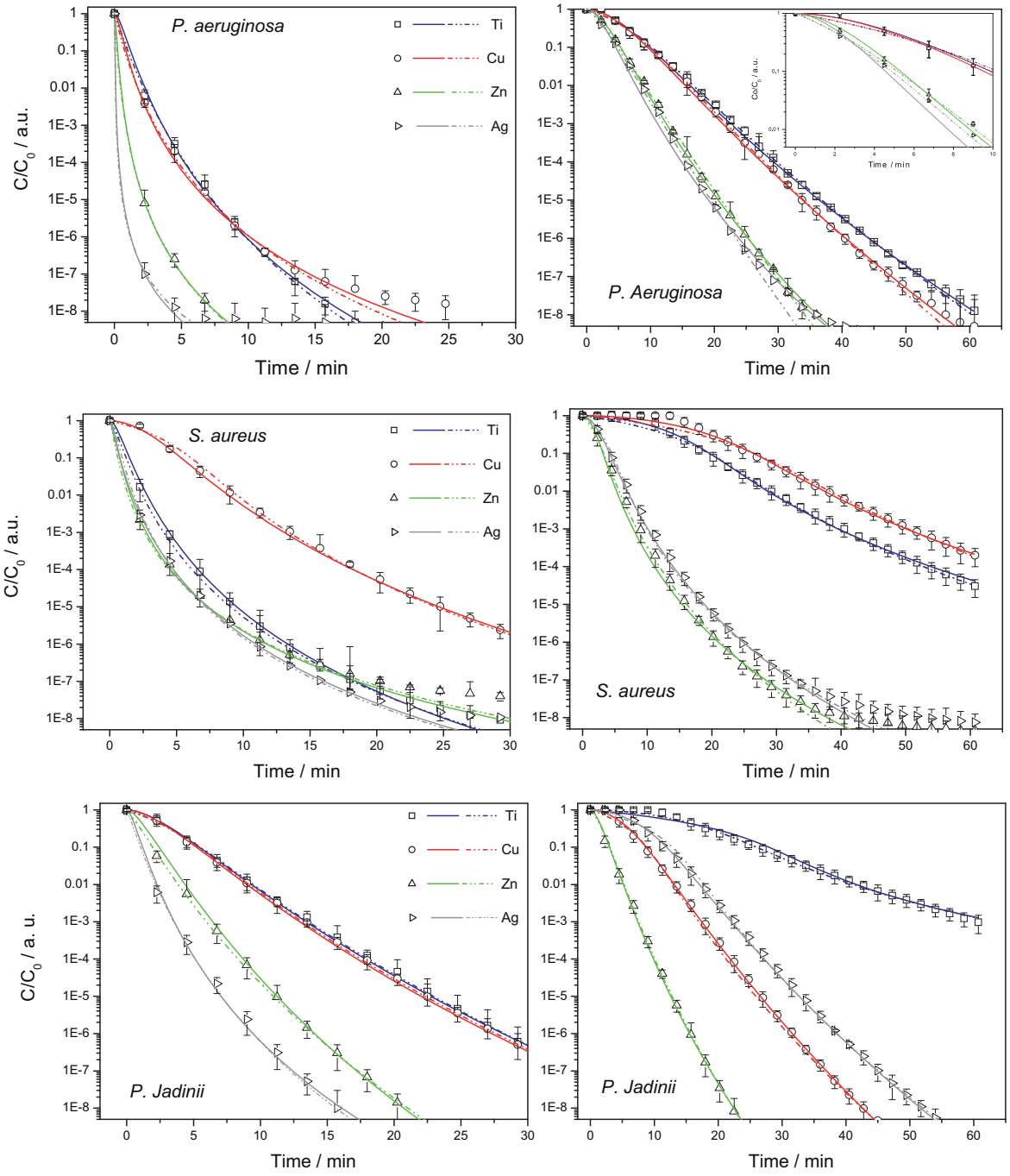

Fig. 1. Elimination profiles (scattered data) and kinetic modeling (dash line, Model 1; full line, Model 2) for Gram-negative (*P. aeruginosa*) and Gram-positive (*S. aureus*) bacteria and a yeast (*P. jadinii*) under UV (left) and visible (right) light excitation.

semicrystalline polymer), relatively invariant throughout the series of samples analyzed.

Results for representative Gram-negative, Gram-positive and yeast microorganisms of our series of pathogens are presented in Fig. 1. Such figure does not display blank experiments as they showed the absence of killing (less than 0.5 log CFU mL^{-1} at the end of the experiment) due to the very low irradiation power used in the experiments. This has been discussed in larger detail by the authors for similar experiments with TiO_2 polymer-oxide composites [5]. Fig. 1 also presents results for the modeling work using what we called here Models 1 and 2. As previously noted, the utilization of an "adsorption Langmuir–Hinshelwood" type mechanism allows a reasonable and relatively flexible description of the inactivation. Moreover, the advantage of using this approach appears two-fold: first, (i) its usefulness in analyzing complete sets of inactivation profiles showing (or lacking) initial smooth/fast decays and final tailing section; additionally, (ii) the model renders kinetic parameters allowing physical interpretation of the underlying process, in contraposition with many other simple kinetic laws used previously [1b,11].

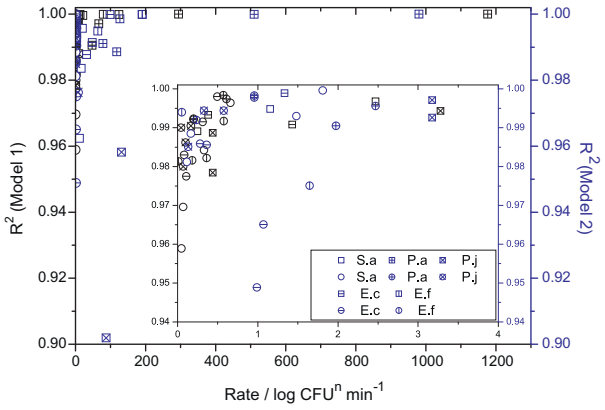

Fig. 2. Goodness of the fit (as measured by the R^2 coefficient) vs. reaction rate for all experiments analyzed. Values are the average of 4 experimental data sets carried out for each the 10 independent experiments presented in this work. Inset: low reaction rate zone detail. Squares, UV data; circles, visible light data. Legend inside the inset describes the symbols used for each microorganism and light excitation.

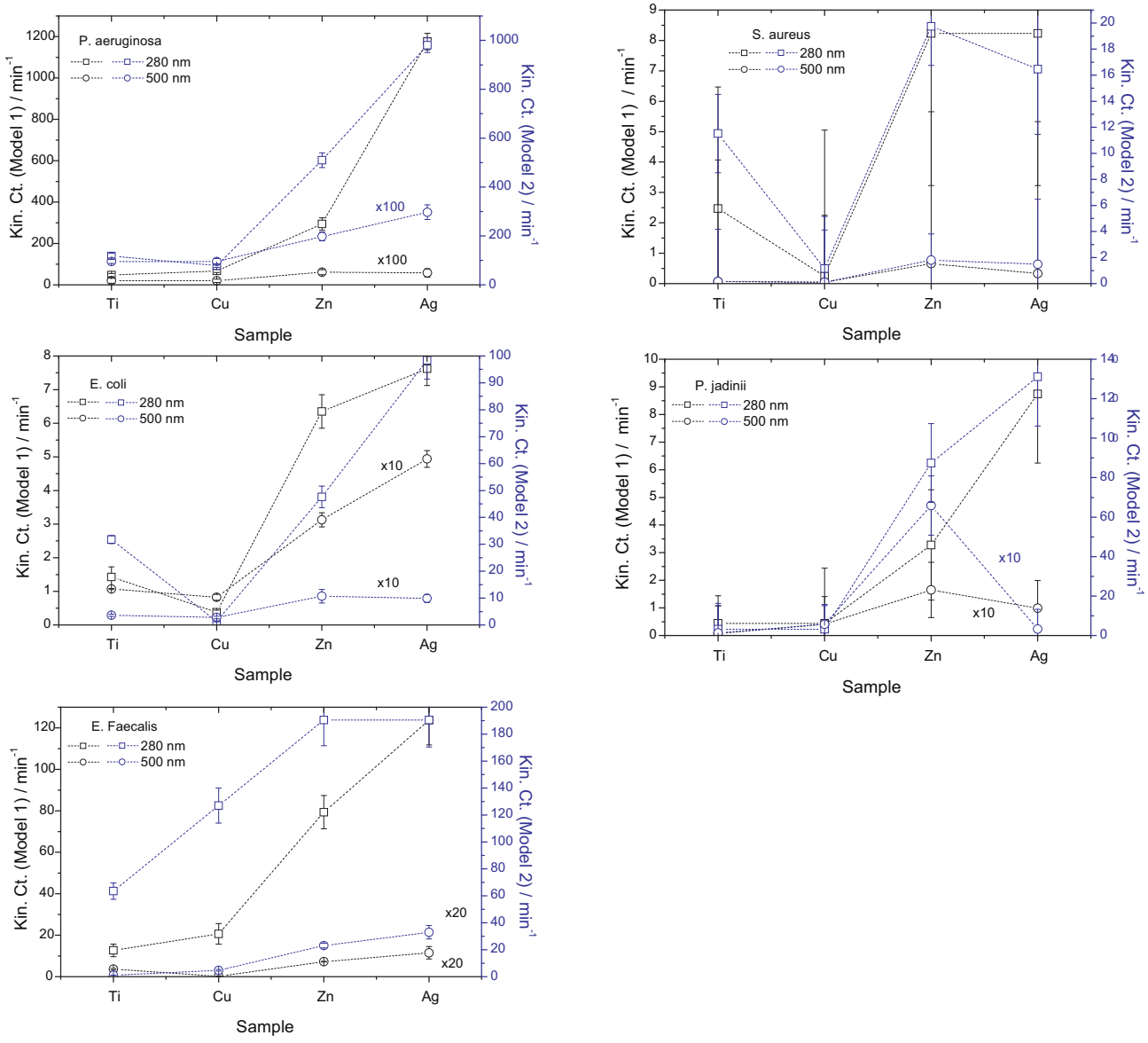

Fig. 3. Kinetic constants obtained from the kinetic analyses displayed in Fig. 1.

Note, in any case, that the complexity of the photo-activated disinfection process occurring once a microbe is in contact with a photogenerated radical means that we can talk of a "adsorption Langmuir–Hinshelwood" type mechanism where the complex set of elemental steps describing the process is crudely approximated by two (Model 2) or one (Model 1) simple uni-molecular elementary reactions. In passing we also like to point out that using polymer-based film erases one of the problems inherent to photocatalytic powders and coming from the phagocytosis of the powder and the subsequent internal effects produced by the oxide. Here only pure radical forms (more precisely those derived from hole charge carriers—see below) escape the nano-composite films [3,5]. We thus have a simple situation with respect to that of photoelimination processes triggered by TiO_2 powders.

Fig. 1 shows results of the biocidal tests in selected cases. The presence of initial shoulders (very weak or even inexistent under UV excitation possibly due to the combined effect of the relative small dead volume of the experiments and the high activity of the samples) and/or tailing final regions is evident in the majority of cases. The fitting results displayed in Fig. 1 provide evidence of the goodness of the models which adequately describe the experimental data, including the mentioned initial shoulders and/or final tailing regions. It may be, however, noted that the model is not able to completely describe tailing regions. In spite of this, rather high values of the coefficient of determination R^2 are obtained. Fig. 2 shows the R^2 values as a function of the reaction rate. Note that measuring the goodness of the fit of a variable spreading across several orders of magnitude using the R^2 coefficient has an undesired skewed originated from the larger weight of the initial points. This likely rationalizes the worsening of the fitting at the tailing region. Fig. 2 indicates the presence of three main regions. At "low" reaction rates, present in the expanded view included in Fig. 2, both models present a similar behavior although the average R^2 value is slightly higher for Model 2 (0.987 ± 0.008 for Model 1 and 0.989 ± 0.009 for Model 2). A simple look of Fig. 2 also shows an intermediate region with rates in the $4\,min^{-1} < rate < 200\,min^{-1}$ zone where Model 1 describes with higher confidence the experimental results. The differential behavior of Models 1 and 2 in these two regions is an expected result, indicating the lower significance of an intermediate "damaged" state as the reaction rate increases or, in other words, in the second with respect to the first region. Of course, the boundary between regions is arbitrary but seems reasonable that a better representation of the "low"/"high" reaction rate region can be achieved using Model 2/1. Finally, there is a third region where the very fast kinetics is fitted with rather high R^2 values (>0.999999) and the fitting model adequacy cannot be discriminated.

Fig. 3 presents the kinetic constants obtained using fitting Models 1 and 2. First to note is that both models give similar trend in almost all cases studied; 5 microorganisms using two light excitations; e.g. 10 independent tests. This makes obvious that discussion of results would be thus based on trends rather than specific values of the kinetic constant values. We also like to briefly mention that the understanding of the differences between Models 1 and 2 parameters numerical values is straightforward if we recall the equations presented in Section 2. Model 2 will always generates higher kinetic constant values while significantly lower differences are expected in the other two parameters. Such numerical differences does not perturb, however, the fact that both models render similar trends providing a tool to test the consistency of the results.

For all microorganisms and irrespective of their nature (Gram negative or positive bacteria and yeast) we found that Zn- and Ag-containing systems perform better than Cu-containing and TiO_2-alone film materials (Fig. 3). Moreover, Cu-containing materials frequently show a worsening of the performance with respect to TiO_2-alone containing films in the *E. coli*, *P. aeruginosa* and *S. aureus* cases. As previously demonstrated this cannot be grounded in significant physico-chemical and, particularly, morphological (e.g. dispersion) properties of the oxide component on the polymer-based composites [10]. Table 1 indicates a moderate beneficial effect in oxide dispersion for Ag- and Zn-containing films and a larger one for the Cu-containing material with respect to the TiO_2 reference film. This trend does not correlate with the photo-killing activity, which thus seems grounded in other physico-chemical properties. As described below, of particular importance in this respect would be the charge handling capability of the materials after light excitation.

Speaking first about UV excitation results and considering valence and conduction band positions in nanosized materials [13], while the CuO_x–TiO_2 contact will withdraw holes from TiO_2, Ag will withdraw electrons (from TiO_2) and ZnO will donate holes to the TiO_2 component. Due to the fact that photo-killing in polymer-based materials as EVOH is expected to proceed trough hole-related species [5], the order of activity seems reasonably explainable and justify the $Cu < TiO_2 \ll Zn < Ag$ general sequence of activity. This is corroborated here using EPR. Absence of oxygen-related radicals photo-generated at the surface of the materials was here observed in presence of oxygen gas phase, in agreement with previous reports of TiO_2-containing polymer films [14]. On the contrary, Fig. 4 displays an example of the signal with 1:2:2:1 intensity pattern observed for all samples in presence of a hole trapping probe molecule (DMPO). Its EPR parameters ($g = 2.0056$, $a_N = 14.9$ G,

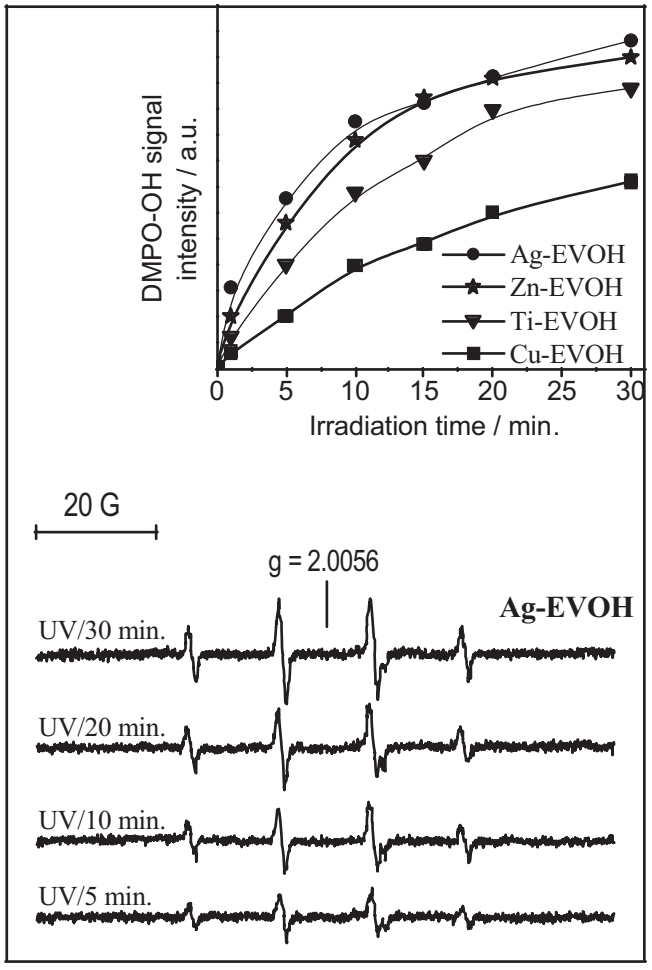

Fig. 4. (A) EPR spectra under UV-light irradiation of the DMPO-OH signal obtained after different time intervals in presence of the Ag-containing thin film. (B) Evolution of the DMPO-OH signal intensity for the samples studied as a function of irradiation time.

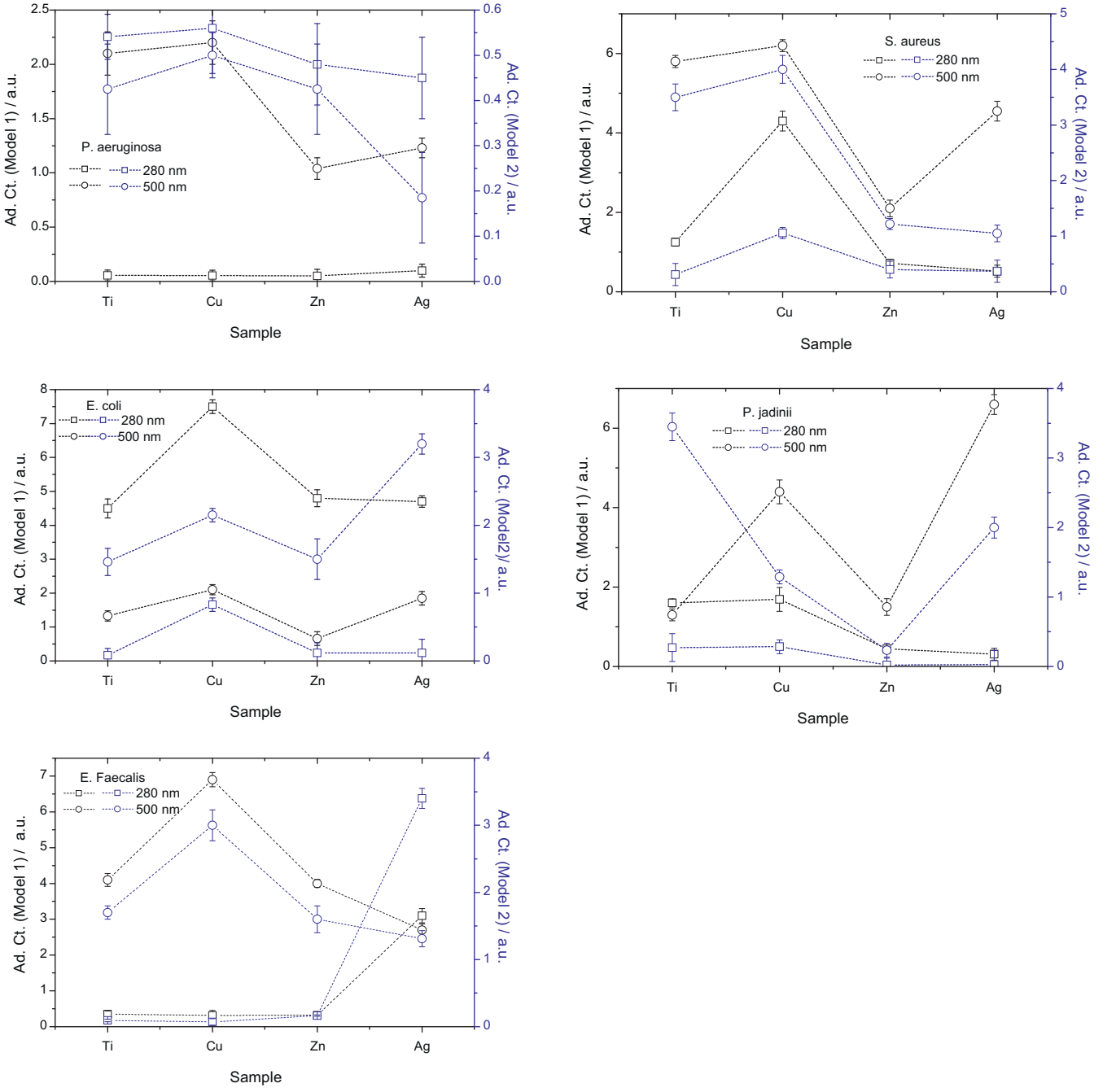

Fig. 5. Adsorption constants obtained from the kinetic analyses displayed in Fig. 1.

a_H = 14.9 G) are characteristic of DMPO-OH adducts [15–18]. The intensity of the DMPO-OH adduct signal as a function of the time under UV irradiation is plotted in the inset of Fig. 4. The accumulation of DMPO-OH radical adducts seems to grow continuously in all cases but a pseudo-steady state is reached toward the end of the experiment. The latter is likely an effect of multiple additions, within consecutive reactions, of OH radicals to DMPO molecules to yield diamagnetic species [13–16]. Differences among samples could be thus mostly analyzed in terms of the initial slope of the curves and directly reflects differences in hole handling properties. We can therefore provide a direct evidence of the existent link between the hole handling properties of the nanocomposites and their photocatalytic disinfection capability. This justifies the already mentioned $Cu < TiO_2 \ll Zn < Ag$ general sequence of activity.

More difficult is the analysis of results upon visible light excitation as the nanocomposite system present its own electronic states (e.g. interface states) not present in the isolated oxide or polymer parent systems [3,5]. In this case of DMPO-OH radical adducts were detected but signal was typically so weak that numerical integration is rather poor. We observed, in any case, a larger quantity of radicals in the Ag-containing sample. This result clearly points out the difficulty of predicting or rationalizing this point as the information on interface states and the subsequent generation of radical species upon light excitation is rather difficult to obtain. In principle and neglecting such interface effect, visible light excitation is only possible in the case of Cu- and Ag-containing materials. However, these two films present rather dissimilar behavior and again a larger similarity is observed between Zn- and Ag-containing materials. This would point out again that the role of interface effects

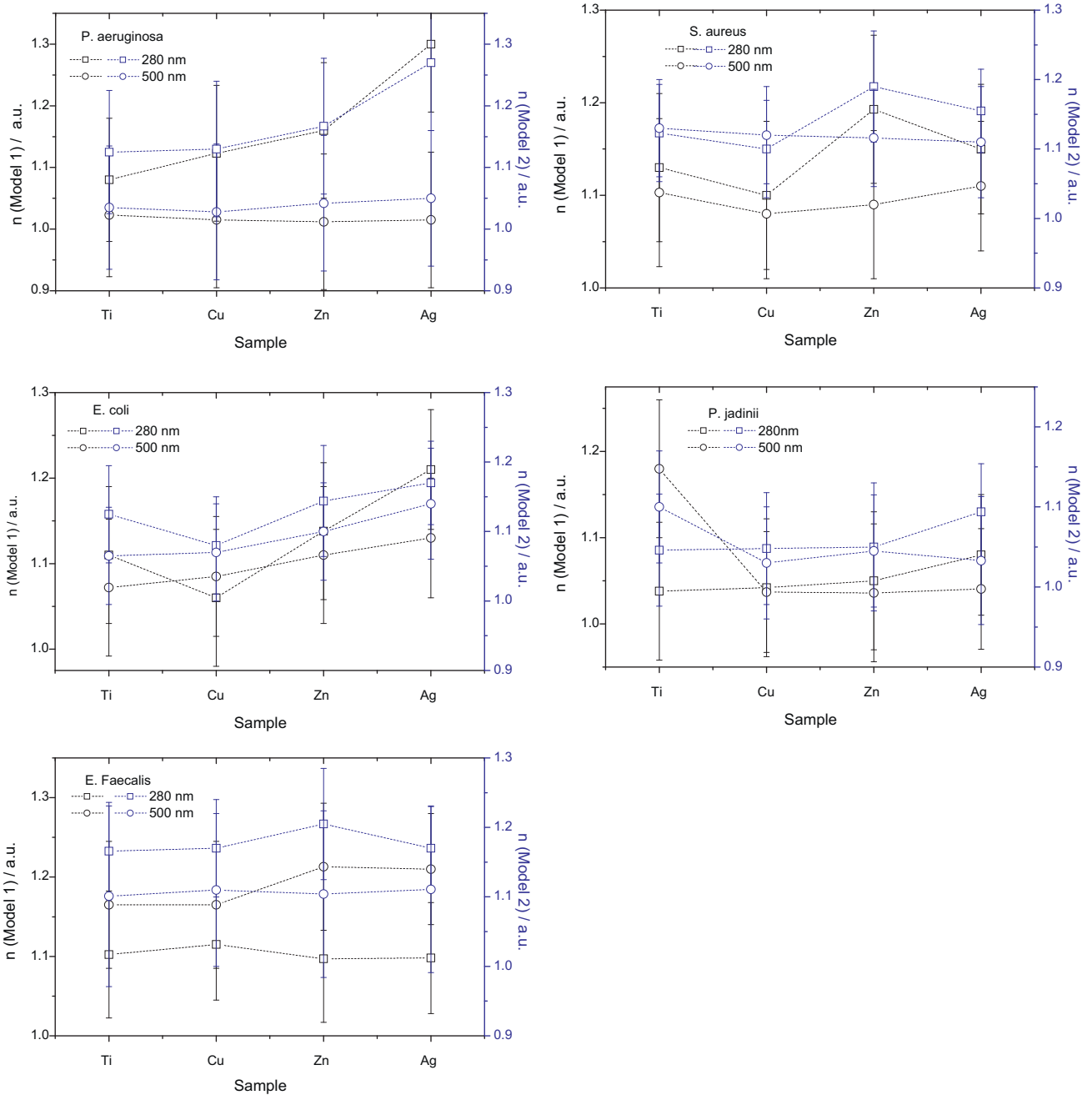

Fig. 6. Exponent coefficients obtained from the kinetic analyses displayed in Fig. 1.

is rather important and may drive the photo-killing behavior upon visible excitation. Obviously, the activity upon visible light is rather moderate if compared to the one upon UV light; however, is not negligible and in the best cases (*E. coli*, *S. aureus* and *P. Jadinii*) the reaction rate is only one order of magnitude lower.

Concerning the nature of the radical attack to the microorganism we carried out a simple dark re-growth experiment after the visible light experiment for TiO_2- and Ag-containing films for a period of 3 h. We did not find any significant evidence of re-growth for both samples (factor increase below 1.2), being such result in line with previous works [19]. This suggests the essentially irreversible nature of the photo-killing process.

Another important issue derived from the study concerns the comparison among the series as a function of the microorganism nature. We can see that we found consistently, both in the Gram-negative and Gram-positive bacteria cases, high and low reaction rates for specimens of each of these two classes of microorganisms and irrespective of the light wavelength (Fig. 1). This clearly indicates that the cell wall degradation could not be the single key step in the inactivation of the microorganism. This is indicated by the comparative analysis with results concerning the photo-elimination of the yeast, a more complex microorganism. Again, the influence of the cell wall seems rather limited to describe the performance of the photo-elimination not only within bacteria but generally speaking in the microorganism word. Note that this happens in systems where no phagocytosis or any subsequently related internal damage must be claimed. So, this would indicate that other key biological components of the microorganisms are damaged more quickly or, at least, in parallel to the cell wall. In this context, metabolic collapse (and cell death), may occur as a

result of radical inactivation of cellular proteins, probably induced by oxidative thiol modifications in vivo [20], that in turns involves rapid collapse of pathways for the synthesis of macromolecules and their precursors with half lives of the cognate enzymes of only a few seconds. Further studies will be required to monitor the temporal overview of the key events in metabolic collapse of the organisms herein analyzed dying in response to radical-induced oxidative damage. Whatever the case, some reports indicate that respiratory systems involved in ATP synthesis [21], nucleic acid [22], and catalytic component such as coenzymes [1b] can fail almost immediately after the initial steps of the radical interaction with the cell and this may limit cell viability. Our results may, however, represent a singular case, specific for polymer-based systems, due to the production of toxic byproducts (related to the polymer part of the thin films) that may damage microorganisms in different or specific ways en each case here studied. We tested the hypothetical presence of such products with EPR but failed to detect them. So, it may be that these hypothetical chemical products are not radical species.

In Figs. 5 and 6 we depict, respectively, the adsorption constants and inhibition coefficients obtained. As previously mentioned in the seminal work of Marugan et al., due to the size of the microorganism, the adsorption constant would generically represent an interaction phenomenon and, properly speaking, not a adsorption steps [11]. In any case, we typically observed that Cu-containing films and, in some cases, Ag-containing films show the highest values of the coefficient. We may think that, in these two systems, the surface of the polymer is possibly the most degraded but, as said, previously, by effect of different charge carrier species. The degradation of the polymer substrate leads to hydrophilic (mostly OH and CO groups) species [3] which may increase the interaction with the microorganisms. We tried to test the degradation of the polymer by thermogravimetry but the differences among samples fell below the detection limit due, mainly, to a combination of the rather low amount (forced by the disinfection experiments) of sample used and the soft changes expected under reaction. Also, ATR (attenuated total reflection) experiments were not able to detect significant changes in the films. The analysis of the adsorption coefficient (Fig. 5) would in any case indicate that these two systems suffer the most important flow of charge carrier species toward the surface of the nanocomposite although in the Cu-case this is not leading to an effective inactivation of the microorganism due to the nature of the main charge carrier reaching the nanocomposite surface [23].

Finally, Fig. 6 presents the inhibition coefficient behavior of the film materials studied. This parameters accounts for the inhibition produced by the increasing concentration of cell debris and oxidation products appearing toward the end of the experiment and competing strongly for the radical species effectively eliminating microorganism. This effect leads to the typical tailing effect observed in Fig. 1 in some cases. The n coefficient is inherently higher than 1 and the larger the difference from this value the acute is the inhibition phenomenon. Here, relatively similar coefficients (around 1.15) for *P. aeruginosa*, *E. coli*, *E. faecalis*, and *S. aureus* microorganisms were encountered irrespective of the energy of the irradiation field although slightly higher values are observed upon UV, consistently with the fact that the disinfection process typically progresses further in this last case with respect to the visible light triggered inactivation. *P. jadinii* displayed the lower average values for this parameter and may indicate a different nature of the photo-killing process, more visible toward the end of the tests.

4. Conclusions

Summing up, the kinetic analysis and particularly the reaction rates and kinetic constants obtained demonstrate that Zn- and Ag-promotion of the TiO_2-based biocidal activity of polymer thin films is rather effective both upon UV and visible light excitations. In the first case (UV) and as showed by electron paramagnetic resonance, the promotion seems intimately related to a beneficial effect directly derived from an optimum handling of the holes produced in the titania phase, while in the second (visible light) the organic–inorganic interface handling of charge carriers seems of prime importance. The results using 5 microorganisms suggest that although initially the radical attack proceeds on the cell wall, the parallel degradation of other cell systems can be of importance in interpreting the disinfection capability of the TiO_2-polymer films. This may be a specific case for polymer-based materials and requires further study.

Acknowledgements

Financial support (CTQ2010-14872/BQU, PLE2009-0037, PRPPRI-PIBJP-2011-0914) is fully acknowledged. A.K. thanks the MICINN program "Ramón y Cajal" for a postdoctoral fellowship. Dr. Marta Fernández García is also thanked for provision of the films.

References

[1] (a) O. Carp, C.L. Huisman, A. Reller, Progress in Solid State Chemistry 32 (2004) 33–177;
(b) O.K. Dalrymple, E. Stefanakos, M.A. Trozt, D.Y. Goswany, Applied Catalysis B 98 (2010) 27–38;
(c) P.S.M. Dunlop, C.P.S. Sheeran, J.A. Bryne, M.A.S. McMahon, M.A. Boyle, K.G. McGuigan, Journal of Photochemistry and Photobiology A 216 (2010) 303–310;
(d) H. Kong, J. Song, J. Jang, Environmental Science and Technology 44 (2010) 5672–5676;
(e) T.V. Duncan, Journal of Colloid and Interface Science 363 (2011) 1–24;
(f) H.A. Foster, I.B. Ditta, S. Varghese, A. Steele, Applied Microbiology and Biotechnology 90 (2011) 1847–1868.
[2] (a) A. Mitoraj, M. Jańczyk, H. Strus, G. Kisch, P.B. Stochel, W. Heczko, W. Macyk, Photochemical and Photobiological Sciences 6 (2007) 642–648;
(b) J.A. Rengifo-Herrera, E. Mielczarski, J. Mielczarski, N.C. Castillo, J. Kiwi, C. Pulgarin, Applied Catalysis B: Environmental 84 (2008) 448–456;
(c) C. Karunakaran, A. Vijayabalan, G. Manikandan, P. Gomathisankar, Catalysis Communications 12 (2011) 826–829;
(d) S. Sontakke, J. Modak, G. Madras, Chemical Engineering Journal 165 (2010) 225–233.
[3] A. Kubacka, C. Serrano, M. Ferrer, H. Lünsdorf, P. Bielecki, M.L. Cerrada, M. Fernández-García, M. Fernández-García, Nano Letters 7 (2007) 2529–2534.
[4] Y. Wang, M. Zhong, F. Chen, J. Yang, Applied Catalysis B 90 (2009) 249–254.
[5] M.L. Cerrada, C. Serrano, M. Sánchez-Chaves, F. Fernández-Martín, A. de Andrés, R. Jiménez-Riobóo, M. Fernández-García, A. Kubacka, M. Ferrer, M. Fernández-García, Advanced Functional Materials 18 (2008) 1949–1960.
[6] P.V. Kamat, Journal of Physical Chemistry C 111 (2007) 2834–2860.
[7] (a) A. Kubacka, A. Martinez-Arias, M. Ferrer, M. Fernández-García, Applied Catalysis B 84 (2008) 87–93;
(b) A. Kubacka, C. Serrano, M.L. Cerrada, M. Fernández-García, M. Ferrer, M. Fernández-García, Journal of Physical Chemistry C 113 (2009) 9182–9190;
(c) R. van Grieken, J. Marugan, C. Sordo, P. Martínez, R. Pablos, Applied Catalysis B 93 (2009) 112–118;
(d) R. Vinu, G. Madras, Applied Catalysis A 366 (2009) 130–140;
(e) A. Emamifar, M. Kadivar, M. Shahedi, S. Soleimanian-Zad, Food Control 22 (2010) 408–413;
(f) D. Wodka, E. Bielaniska, R.P. Socha, M. Elzbieciak-wodka, J. Gurgul, P. Nowak, P. Warszynxki, I. Kumariki, ACS Applied Materials and Interfaces 9 (2010) 1945–1953;
(g) J. Ma, Z. Xiong, D. Waite, W.J. Ng, X.S. Zhao, Microporous and Mesoporous Materials 144 (2011) 97–104;
(h) J. Thomas, K.P. Kumart, K.R. Chitra, Advanced Science Letters 4 (2011) 108–114;
(i) I. Piwonski, K. Kdzola, A. Kisielewska, A. Soliwoda, M. Wolszczak, M. Lisowska, N. Wronska, A. Felczak, Applied Surface Science 257 (2011) 7076–7082;
(j) L. Liu, Z. Liu, H. Bai, D.D. Sun, Water Research 46 (2012) 112–118.
[8] (a) M.K.I. Senevirathna, P.K.D.D.P. Pitigala, K. Tennakone, Journal of Photochemistry and Photobiology A 171 (2005) 257–269;
(b) A. Torres, C. Ruales, C. Pulgarín, A. Aimable, P. Bowen, V. Sarria, J. Kiwi, ACS Applied Materials and Interfaces 2 (2010) 2547–2552.
[9] (a) D. Chen, H. Zhang, S. Hu, J. Li, Journal of Physical Chemistry C 112 (2008) 117–122;
(b) C. Karunakaran, G. Abiramar, P. Gomathisankar, G. Manikandan, V. Anandi, Materials Research Bulletin 46 (2011) 1586–1592;

(c) S.H. Hwang, J. Song, Y. Jung, O.Y. Kweon, H. Song, J.H. Jang, Chemical Communications 47 (2011) 9164–9166.
[10] A. Kubacka, M. Ferrer, M.L. Cerrada, C. Serrano, M. Fernández-García, M. Fernández-García, Applied Catalysis B 89 (2011) 441–449.
[11] J. Marugán, R. van Grieken, C. Sordo, C. Cruz, Applied Catalysis B 82 (2008) 27–36.
[12] J.E. Dennis, D.M. Gay, R.E. Welsh, ACM Transactions of Mathematical Software 7 (1981), 348–368, 369–383.
[13] A. Kubacka, M. Fernández-García, G. Colón, Chemical Reviews 112 (2012) 1555–1614.
[14] A. Kubacka, M. Ferrer, M.L. Cerrada, C. Serrano, M. Sánchez-Chaves, A. de Andrés, R. Jiménez-Riobóo, M. Fernández-García, F. Fernández-Martín, M. Fernández-García, Applied Catalysis B 89 (2009) 441–447.
[15] M. Che, A. Tench, Journal of Advanced Catalysis 32 (1983) 1–69.
[16] Y. Nakaoka, Y. Nosaka, Journal of Photochemistry and Photobiology A 110 (1997) 299–307.
[17] E.G. Janzen, N. Sankuratry, Y. Kotake, Journal of Magnetic Resonance 111 (1996) 254–263.
[18] M.D. Hernández-Alonso, A.B. Hungría, A. Martínez-Arias, M. Fernández-García, J.M. Coronado, J.C. Conesa, J. Soria, Applied Catalysis B 50 (2004) 167.
[19] D. Wu, H. You, D.J. Xu, Journal of Photochemistry and Photobiology A 217 (2011) 177–183 (And references therein).
[20] L.I. Leichert, F. Gehrke, H.V. Gudiseva, T. Blackwell, M. Ilbert, A.K. Walker, J.R. Strahler, P.C. Andrews, U. Jakob, Proceedings of the National Academy of Sciences of the United States of America 105 (2008) 8197–8202.
[21] C.-N. Lok, et al., Journal of Proteome Research 5 (2006) 916–924.
[22] G. Gogniat, S. Dukan, Applied and Environment Microbiology 73 (2007) 7740–7743.
[23] B.E Logan, B. Hamelers, R. Rozendal, U. Schroder, J. Keller, W. Verstraete, K. Rabaley, Environmental Science and Technology 40 (2006) 5181–5185.